Mon. Not. R. Astron. Soc. **344,** 696–706 (2003)

Inner-shell photoexcitation of Fe XV and Fe XVI

R. Kisielius,[1★†] A. Hibbert,[2] G. J. Ferland,[3] M. E. Foord,[4] S. J. Rose,[5]
P. A. M. van Hoof[1] and F. P. Keenan[1]

[1]*Department of Pure and Applied Physics, Queen's University of Belfast, Belfast BT7 1NN*
[2]*Department of Applied Mathematics and Theoretical Physics, Queen's University of Belfast, Belfast BT7 1NN*
[3]*Department of Physics, University of Kentucky, Lexington, KY 40506, USA*
[4]*University of California, Lawrence Livermore National Laboratory, Livermore, CA 94551, USA*
[5]*Department of Physics, Clarendon Laboratory, Parks Road, Oxford OX1 3PU*

Accepted 2003 May 14. Received 2003 May 13; in original form 2003 March 16

ABSTRACT

The configuration-interaction method as implemented in the computer code CIV3 is used to determine energy levels, electric dipole radiative transition wavelengths, oscillator strengths and transition probabilities for inner-shell excitation of transitions in Fe XV and Fe XVI. Specifically, transitions are considered of the type $1s^2 2s^2 2p^6 3s^2$–$1s^2 2s^2 2p^5 3l 3l' 3l''$ (l, l' and l'' = s, p or d) in Fe XV and $1s^2 2s^2 2p^6 3s$–$1s^2 2s^2 2p^5 3l 3l'$ (l and l' = s, p or d) in Fe XVI, using the relativistic Breit–Pauli approach. An assessment of the accuracy of the derived atomic data is performed.

Key words: atomic data – line: formation – X-rays: general.

1 INTRODUCTION

As a result of the launch of the *XMM–Newton* and *Chandra* satellites, new high-resolution X-ray astronomical spectra are becoming widely available. Both emission and absorption X-ray spectra originating from various astrophysical objects, such as accretion disc in active galactic nuclei (AGN), X-ray binary stars, neutron stars, X-ray pulsars, supernova remnants, X-ray emitting shocks and the interstellar ionized medium, have been recorded and studied (see, for example, Kaspi et al. 2000; Yang, Wilson & Ferruit 2001; Ballantyne, Ross & Fabian 2002; Schurch & Warwick 2002). Along with these observations, the X-ray emission and absorption spectra from laboratory sources, such as the Sandia National Laboratory *Z*-pinch facility, have been reported recently (Foord et al. 2001).

For the reliable interpretation of high-resolution X-ray spectroscopic observations, one needs accurate atomic data describing various fundamental processes that determine the ionization structure, the electron temperature, the level population of excited states and emission/absorption line properties, such as wavelengths or intensities of highly charged ions which are abundant in the observed sources. These atomic data are employed in spectral modelling codes such as GALAXY (Rose 1998), CLOUDY (Ferland et al. 1998), XSTAR (Kallman & Bautista 2001).

A very large number of absorption lines belonging to different charge states of iron ions are present in the X-ray spectra obtained from observed astrophysical objects. Some recent efforts to generate absorption soft X-ray spectra of the 16 Fe charge states for inner-shell ($n = 2$) photoexcitation was reported by Behar, Sako & Kahn (2001), where a relativistic approach was used to calculate the wavelengths and oscillator strengths for the radiative transitions from the inner 2p and 2s shells, along with autoionization transitions.

In the present work we employ the configuration-interaction (CI) code CIV3 (Hibbert 1975) to determine the wavefunctions of the ions considered. The method of superposition of configurations applied here is capable of producing very accurate data for this type of calculation, which requires high levels of correlation. Relativistic effects are introduced by adding Breit–Pauli operators into the Hamiltonian (Hibbert, Glass & Froese Fischer 1991). Combining these two methods, we can reliably determine *LSJ*-energy levels, absorption oscillator strengths and emission transition probabilities for the electric dipole (E1) 2p–3*l* transitions between fine-structure levels.

2 METHOD OF CALCULATION

In a CI calculation, the atomic-state wavefunction is represented in the form of a linear superposition of configuration-state functions (CSFs). In the non-relativistic (*LS*) approximation, this can be expressed as

$$\Psi(LS) = \sum_i a_i \Phi_i(\alpha_i LS), \tag{1}$$

where Φ_i represents a set of CSFs that possess the same total $LS\pi$ symmetry. In the case of the Breit–Pauli approximation, this changes to

$$\Psi(J) = \sum_i a_i \Phi_i(\alpha_i L_i S_i J), \tag{2}$$

★E-mail: R.Kisielius@qub.ac.uk
†On leave of absence from: Institute of Theoretical Physics and Astronomy, A. Goštauto 12, Vilnius 2600, Lithuania.

where the CSFs represent several different *LS* terms, each of which has the same J value and parity π. In each case the set of CSFs $\{\Phi_i\}$ is constructed as normalized antisymmetric products of the one-electron function, the angular momenta of which are coupled in a manner denoted by $\{\alpha_i\}$, such that the resultant is an eigenfunction of the total angular momentum operators $\{\boldsymbol{L}^2, \boldsymbol{S}^2\}$ for the *LS*-coupling or $\{\boldsymbol{J}^2\}$ for the intermediate *LSJ*-coupling. The coefficients $\{\alpha_i\}$ correspond to an eigenvector of the Hamiltonian matrix with particular symmetry ($LS\pi$ or $J\pi$).

In order to determine wavefunctions using the *LS*-coupling scheme of the CI expansion, we use the Hamiltonian constructed solely from the Schrödinger non-relativistic operator, while in the relativistic case we use this operator plus the spin–orbit operator, the spin–other–orbit operator, the spin–spin operator, the mass–correction operator and the Darwin term. The orbit–orbit interaction, although more significant for inner-shell excitation than for outer-shell transitions, remains small compared with the degree of accuracy which can be achieved for E1-transition wavelengths.

The configuration state functions used in equations (1) and (2) are constructed from a set of one-electron orbitals for which the radial part is presented by a linear combination of normalized Slater-type orbitals χ_{jnl}:

$$P_{nl}(r) = \sum_{j=1}^{k} c_{jnl}\,\chi_{jnl}(r), \tag{3}$$

where

$$\chi_{jnl}(r) = \frac{(2\zeta_{jnl})^{I_{jnl}+1/2}}{[(2I_{jnl})!]^{1/2}} r^{I_{jnl}} \exp(-\zeta_{jnl} r). \tag{4}$$

In our approach radial one-electron orbitals must satisfy the orthonormality conditions

$$\int_0^\infty P_{nl}(r) P_{n'l}(r)\,\mathrm{d}r = \delta_{nn'}. \tag{5}$$

The parameters c_{jnl} and ζ_{jnl} in equations (3) and (4) are determined by the CIV3 code using an optimization procedure for the eigenvalues of the non-relativistic Hamiltonian.

2.1 Radial functions

We need to obtain wavefunctions of Fe XVI and Fe XV that are as accurate as possible for all states under investigation. Initially, we choose the 1s, 2s, 2p and 3s radial orbitals as the Hartree–Fock functions. Consequently, we can use their parameters given by Clementi & Roetti (1974). With these core orbitals, the radial orbital parameters for 3p and 3d functions were obtained using the CIV3 code.

In Fe XVI we study electric dipole transitions from the ground $1s^2 2s^2 2p^6 3s$ configuration to the configurations $1s^2 2s^2 2p^5 3l 3l'$, where l and l' can be any of the s, p or d orbitals. Consequently, we optimize the 3p orbital functions on the lowest ^{2}P term of the $2p^5 3s3p$ configuration. Similarly, we optimize 3d orbital functions on the lowest ^{2}P term of the $2p^5 3s3d$ configuration. In both procedures, we use a single-configuration approach, which gives only two CSF, producing ^{2}P terms.

In addition to valence orbitals $3l$, we use 'correlation' orbitals denoted by $\bar{4}l$ in order to improve the accuracy of wavefunctions. The optimization of their parameters was performed in the following way. The $\bar{4}$s orbital was optimized on the lowest ^{2}P term of the $2p^5 3s3d$ configuration using the configurations $2p^5 3s3d$, $2p^5 3d^2$ and $2p^5 3s\bar{4}s$. The $\bar{4}$p orbital was optimized on the lowest ^{2}P term of the $2p^5 3p^2$ configuration using the configurations $2p^5 3p^2$, $2p^5 3s3d$, $2p^5 3p\bar{4}p$ and $2p^5 \bar{4}p^2$. The $\bar{4}$d orbital was optimized on the lowest ^{2}P term of the $2p^5 3s3d$ configuration using the configurations $2p^5 3s3d$, $2p^5 3d^2$, $2p^5 3s\bar{4}d$ $2p^5 3d\bar{4}s$ and $2p^5 \bar{4}d^2$. The $\bar{4}$f orbital was optimized on the lowest ^{2}P term of the $2p^5 3p^2$ configuration using the configurations $2p^5 3p^2$, $2p^5 3s3d$, $2p^5 3p\bar{4}f$ and $2p^5 \bar{4}f^2$. The optimized parameters c_{jnl} and ζ_{jnl} and the values of I_{jnl} used in our calculation for each of the orbitals are given in Table 1.

Table 1. Parameters of the Fe XVI and Fe XV radial basis orbitals.

		Fe XVI		Fe XV	
nl	I_{jnl}	c_{jnl}	ζ_{jnl}	c_{jnl}	ζ_{jnl}
3p	2	0.323 92	13.906 85	0.303 51	14.168 13
	3	0.404 49	10.291 56	0.362 21	10.720 46
	3	−1.269 13	5.897 73	−1.214 07	5.722 91
3d	3	0.094 44	10.413 35	0.105 33	10.185 72
	3	0.928 26	5.752 60	0.920 12	5.596 45
$\bar{4}s$	1	0.422 14	18.299 06	0.435 62	17.283 47
	2	−8.295 09	4.744 37	−9.205 59	4.705 63
	3	6.384 04	6.009 08	9.446 03	6.207 82
	4	−0.942 33	6.389 65	−2.655 39	7.339 90
	4	3.006 02	10.555 76	2.488 17	10.029 44
$\bar{4}$p	2	0.157 00	23.973 02	0.548 98	13.235 41
	3	2.007 33	11.183 12	1.215 18	8.580 96
	4	−2.974 88	11.339 20	−2.782 44	9.900 39
	4	1.164 63	5.630 79	1.351 55	5.708 09
$\bar{4}$d	3	2.655 97	6.867 20	1.372 02	8.376 36
	4	−4.348 73	6.346 84	−0.600 14	7.791 86
	4	1.715 44	5.625 32	−0.791 22	4.751 64
$\bar{4}f$	4	4.063 87	5.017 75	1.983 56	5.824 60
	4	−3.149 69	4.652 12	−1.010 81	5.220 16

In Fe XV we consider electric dipole transitions from the ground $1s^2 2s^2 2p^6 3s^2$ configuration to the configurations $1s^2 2s^2 2p^5 3l 3l' 3l''$, where l, l' and l'' can be any of the s, p or d orbitals. Consequently, we choose to optimize 3p orbital functions on a single ^{3}P term of the $2p^5 3s^2 3p$ configuration, and 3d orbital functions on a ^{2}P term of the $2p^5 3s^2 3d$ configuration.

The parameters of 'correlation' orbitals $\bar{4}$s, $\bar{4}$p, $\bar{4}$d, $\bar{4}$f were obtained in a procedure similar to that described above. The $\bar{4}$s orbital was optimized on the $2p^5 3s^2 3d$ ^{3}P term using the configurations $2p^5 3s^2 3d$, $2p^5 3s^2 \bar{4}s$, $2p^5 3s^2 \bar{4}s^2$ and $2p^5 3s3d\bar{4}s$. The $\bar{4}$p orbital was optimized on the lowest $2p^5 3s3p^2$ ^{3}P term using the configurations $2p^5 3s^2 3d$, $2p^5 3p^2 3d$, $2p^5 3s3p^2$, $2p^5 3s\bar{4}p^2$, $2p^5 3s3p\bar{4}p$ and $2p^5 3p3d\bar{4}p$. The $\bar{4}$d orbital was optimized on the $2p^5 3s^2 3d$ ^{1}P term using the configurations $2p^5 3s^2 3d$, $2p^5 3p^2 3d$, $2p^5 3s^2 \bar{4}d$, $2p^5 3p^2 \bar{4}d$ and $2p^5 3s3d\bar{4}d$. The $\bar{4}$f orbital was optimized on the $2p^5 3s^2 3d$ ^{3}P term using the configurations $2p^5 3s^2 3d$, $2p^5 3p^2 3d$ and $2p^5 3p3d\bar{4}f$. The radial orbital parameters c_{jnl}, ζ_{jnl} and I_{jnl} are presented in Table 1.

2.2 Configuration sets

The ground level of the Fe XVI ion is $1s^2 2s^2 2p^6 3s$ $^2S^e_{1/2}$. We chose the CI wavefunction expansion for this level such that no more than two electrons are excited from the 2p and 3s shells. As a result, we include configurations $2p^6 3s$, $2p^5 3s3p$ and $2p^5 3p3d$ with valence orbitals 3s, 3p and 3d, configurations $2p^6 \bar{4}s$, $2p^5 3s\bar{4}p$, $2p^5 3s\bar{4}f$, $2p^5 3p\bar{4}s$, $2p^5 3p\bar{4}d$, $2p^5 3d\bar{4}p$ and $2p^5 3d\bar{4}f$ with one electron within 'correlation' $\bar{4}l$ shell and configurations $2p^5 \bar{4}s\bar{4}p$, $2p^5 \bar{4}s\bar{4}f$, $2p^5 \bar{4}p\bar{4}d$ and $2p^5 \bar{4}d\bar{4}f$ with two valence orbitals. We consider $^2S^e$, $^2P^e$, $^4P^e$ and $^4D^e$ final terms, which can produce levels with the total angular momentum $J = 1/2$. Consequently, we have 94 CSFs in the CI wavefunction expansion of the lower level.

Selection rules for the E1 transition define that we have possible $J = 1/2$ and $3/2$ levels in the upper configuration with the 2p

vacancy. As the configuration itself or *LS* are not exact quantum numbers in the case of relativistic intermediate coupling, we consider all possible transitions from the 2p to the 3*l* shells. In order to keep our calculation consistent, we employ the same basic principles for the CI wavefunction expansion as in the lower configuration case. First of all, we include the configurations under consideration for the transition array, namely $2p^5 3s^2$, $2p^5 3p^2$, $2p^5 3p^2$ and $2p^5 3s3d$. These are supplemented by $2p^6 3p$, $2p^6\bar{4}p$, $2p^5 3s\bar{4}s$, $2p^5 3s\bar{4}d$, $2p^5 3p\bar{4}p$, $2p^5 3p\bar{4}f$, $2p^5 3d\bar{4}s$, $2p^5 3d\bar{4}d$, $2p^5\bar{4}s^2$, $2p^5\bar{4}p^2$, $2p^5\bar{4}d^2$, $2p^5\bar{4}f^2$, $2p^5\bar{4}s\bar{4}d$ and $2p^5\bar{4}p\bar{4}f$ configurations. For the $J = 1/2$ fine-structure levels, we consider the $^2S^o$, $^2P^o$, $^4P^o$ and $^4D^o$ final terms, resulting in 93 configuration state functions. Alternatively for the $J = 3/2$ fine-structure levels, the symmetries considered are $^4S^o$, $^2P^o$, $^4P^o$, $^2D^o$, $^4D^o$ and $^4F^o$ and there are 147 CSFs in a wavefunction expansion.

The ground level of the Fe XV ion is $1s^2 2s^2 2p^6 3s^2\ ^1S^e_0$. We chose all possible configurations with one or no vacancy in the 2p shell and outer electrons distributed in 3*l* and 4*l* shells for the inclusion in the CI wavefunction expansion of this state. This means we have one group of the $2p^6 3s^2$, $2p^6 3p^2$, $2p^6 3d^2$, $2p^5 3s^2 3p$, $2p^5 3p^3$, $2p^5 3p3d^2$, $2p^5 3s3p3d$ configurations with two or three electrons within the $n = 3$ shell. The configurations $2p^6 3s\bar{4}s$, $2p^6 3p\bar{4}p$, $2p^6 3d\bar{4}d$, $2p^5 3s^2\bar{4}p$, $2p^5 3p^2\bar{4}p$, $2p^5 3d^2\bar{4}p$, $2p^5 3d^2\bar{4}f$, $2p^5 3s3p\bar{4}s$, $2p^5 3s3p\bar{4}d$, $2p^5 3p3d\bar{4}s$, $2p^5 3p3d\bar{4}d$, $2p^5 3s3d\bar{4}p$ and $2p^5 3s3d\bar{4}f$ make another group with a single electron excited to the $n = 4$ shell. In addition to that, we include the configurations $2p^6\bar{4}s^2$, $2p^6\bar{4}p^2$, $2p^6\bar{4}d^2$, $2p^6\bar{4}f^2$, $2p^5 3p^2\bar{4}s^2$, $2p^5 3p^2\bar{4}p^2$, $2p^5 3p^2\bar{4}d^2$, $2p^5 3p^2\bar{4}f^2$, $2p^5 3s\bar{4}s\bar{4}p$, $2p^5 3s\bar{4}s4f$, $2p^5 3s\bar{4}p\bar{4}d$, $2p^5 3s\bar{4}d4f$, $2p^5 3p\bar{4}s\bar{4}d$, $2p^5 3p\bar{4}p\bar{4}f$, $2p^5 3d\bar{4}s\bar{4}p$, $2p^5 3d\bar{4}s\bar{4}f$, $2p^5 3d\bar{4}p\bar{4}d$ and $2p^5 3d\bar{4}d\bar{4}f$ with two electrons excited to the $n = 4$ shell. We consider the $^1S^e$, $^3P^e$ and $^5D^e$ terms, which produce $J = 0$ fine-structure levels. Construction of such a basis gives us the 401 CSFs in the CI wavefunction expansion for the lower state of the Fe^{16+} ion.

Because of the electric dipole transition selection rules, we have to consider fine-structure levels with $J = 1$ in the upper state. In the same way as for the lower even state, we make three groups of configurations for the upper (odd) state. The first group consists of the $2p^6 3s3p$, $2p^6 3p3d$, $2p^5 3s^2 3d$, $2p^5 3s3p^2$, $2p^5 3s3d^2$, $2p^5 3p^2 3d$, $2p^5 3d^3$ configurations, which have one or two electrons excited to $n = 3$ shells. The next group is made of the configurations $2p^6 3s\bar{4}p$, $2p^6 3p\bar{4}s$, $2p^6 3p\bar{4}d$, $2p^6 3d\bar{4}p$, $2p^6 3d\bar{4}f$, $2p^5 3s^2\bar{4}s$, $2p^5 3s^2\bar{4}d$, $2p^5 3p^2\bar{4}s$, $2p^5 3p^2\bar{4}d$, $2p^5 3d^2\bar{4}s$, $2p^5 3d^2\bar{4}d$, $2p^5 3s3d\bar{4}s$, $2p^5 3s3d\bar{4}d$, $2p^5 3s3p\bar{4}p$, $2p^5 3p3d\bar{4}f$, $2p^5 3p3d\bar{4}p$ and $2p^5 3p3d\bar{4}f$ with all possible electron distributions having a single electron excited to the $n = 4$ shell. The third group is made of the $2p^6\bar{4}s\bar{4}p$, $2p^6\bar{4}p\bar{4}d$, $2p^6\bar{4}d\bar{4}f$, $2p^5 3s\bar{4}s^2$, $2p^5 3s\bar{4}p^2$, $2p^5 3s\bar{4}d^2$, $2p^5 3s\bar{4}f^2$, $2p^5 3d\bar{4}s^2$, $2p^5 3d\bar{4}p^2$, $2p^5 3d\bar{4}d^2$, $2p^5 3d\bar{4}f^2$, $2p^5 3s\bar{4}s\bar{4}d$, $2p^5 3s\bar{4}p\bar{4}f$, $2p^5 3d\bar{4}s\bar{4}d$, $2p^5 3d\bar{4}p\bar{4}f$, $2p^5 3p\bar{4}s\bar{4}p$, $2p^5 3p\bar{4}s\bar{4}f$, $2p^5 3p\bar{4}p\bar{4}d$ and $2p^5 3p\bar{4}d\bar{4}f$ configurations, which have two electrons in the open $n = 4$ shells. We restricted our set where there could be no more than two electrons in the excited $n = 4$ shell. Here we consider the $^3S^o$, $^1P^o$, $^3P^o$, $^5P^o$, $^3D^o$, $^5D^o$, $^5F^o$ terms, which can produce fine-structure levels with $J = 1$. As a result of this, we have the CI wavefunction expansion with 1065 CSFs for the upper states of the Fe^{16+} ion.

3 RESULTS

3.1 Energy levels

In Table 2 we present the energy levels for the Fe XVI ion calculated using the Breit–Pauli approximation. The energy levels are given in cm^{-1} relative to the ground state $1s^2 2s^2 2p^6 3s\ ^2S_{1/2}$ along with the leading percentage compositions a_i from equation (2) for the 18 excited-state fine-structure levels with $J = 1/2$ and 27 levels with $J = 3/2$. We present only contributions with $a_i^2 \geqslant 0.1$ for this ion.

The leading percentage compositions in Table 2 indicate the strong level of mixing between different *LS* states of the excited upper state, which has a vacancy in the 2p shell. In general, the mixing could be so strong that it would not be possible to make a definite identification of levels represented by that wavefunction. For this reason we do not try to assign fine-structure levels to any *LSJ* quantum numbers. Instead we use a level index to indicate the parity (o for odd or e for even) and *J* to represent the level and E_J the level energy. The leading contributions of wavefunctions depend on the model used, and hence they can differ depending on the calculations or radial orbitals used.

In Table 3 we present the fine-structure energy levels for the Fe XV ion. The energy level values relative to the ground state $1s^2 2s^2 2p^6 3s^2\ ^1S_0$ are given in cm^{-1} for the 87 levels of the excited state with 2p vacancy. The leading percentage compositions are limited to those with $a_i^2 \geqslant 0.07$.

One can note an even stronger configuration mixing for the levels of the Fe XV ion compared with Fe XVI. For the 35^o_1 level, the two largest contributions are as low as 10 per cent. Similarly to the Fe XVI ion case, we cannot assign fine-structure levels in any other way than using a level index with parity and *J* and an energy value.

3.2 Electric dipole transition probabilities and oscillator strengths

After determining the CI wavefunctions Ψ_i for the ground-state fine-structure levels and the wavefunctions Ψ_j for the excited-state fine-structure levels, one can determine the electric dipole transition probabilities (*A*-values) and oscillator strengths (*f*-values). Oscillator strengths can be calculated using both the length (*L*) and velocity (*V*) forms of the E1-transition operator.

The E1 absorption length-form oscillator strength f_L is given by

$$f_L = \frac{2}{3g_i}\Delta E_{ij}\left|\left\langle \Psi_i \left| \sum_{k=1}^{N} \boldsymbol{r_k} \right| \Psi_j \right\rangle\right|^2, \tag{6}$$

and the velocity-form oscillator strength f_V by

$$f_V = \frac{2}{3g_i}(\Delta E_{ij})^{-1}\left|\left\langle \Psi_i \left| \sum_{k=1}^{N} \boldsymbol{\nabla_k} \right| \Psi_j \right\rangle\right|^2, \tag{7}$$

where $g_i = 2J_i + 1$ is the statistical weight of the initial (ground) level and ΔE_{ij} is the transition energy in atomic units. The sum in the transition operator runs over all *N* electrons.

The difference between the results obtained from the length and velocity forms can serve as an indicator of the accuracy of the calculation. Usually, the velocity-form results are more sensitive to the accuracy of the wavefunctions Ψ compared with the length-form data. Hence, although we have performed atomic data calculations for both forms of the transition operator, only the length-form results are presented in our final tables. We use the velocity-form *f*-values for establishing the accuracy of our results, as discussed in the next section.

The length-form electric dipole line emission transition probability A_L (in s^{-1}) is given by

$$A_L = \frac{2.142 \times 10^{10}}{g_j}(\Delta E_{ij})^3\left|\left\langle \Psi_i \left| \sum_{k=1}^{N} \boldsymbol{r_k} \right| \Psi_j \right\rangle\right|^2, \tag{8}$$

Table 2. Energy level indices, their values (in cm^{-1}) relative to the $1^e_{1/2}$ level and configuration contributions of the Fe XVI ion levels with $J = 1/2$ and $3/2$.

Level index	Energy (cm^{-1})	Contributions (in per cent)		
$1^e_{1/2}$	0.00	100, $2p^6 3s\ ^2S$		
$1^o_{1/2}$	5894 438.26	97, $2p^5 3s^2\ ^2P$		
$2^o_{1/2}$	6314 191.40	50, $2p^5(3p^2\ ^1D)\ ^2P$	20, $2p^5(3p^2\ ^3P)\ ^2P$	12, $2p^5(3p^2\ ^3P)\ ^4P$
$3^o_{1/2}$	6350 003.23	60, $2p^5(3p^2\ ^3P)\ ^4P$	20, $2p^5(3p^2\ ^3P)\ ^2S$	12, $2p^5(3p^2\ ^1D)\ ^2P$
$4^o_{1/2}$	6399 342.30	66, $2p^5(3p^2\ ^3P)\ ^4D$	18, $2p^5(3p^2\ ^3P)\ ^2S$	
$5^o_{1/2}$	6415 639.99	97, $2p^5 3s(^3P)3d\ ^4P$		
$6^o_{1/2}$	6435 168.96	56, $2p^5(3p^2\ ^3P)\ ^2S$	25, $2p^5(3p^2\ ^3P)\ ^4P$	17, $2p^5(3p^2\ ^3P)\ ^4D$
$7^o_{1/2}$	6469 208.84	40, $2p^5 3s(^1P)3d\ ^2P$	23, $2p^5(3p^2\ ^3P)\ ^2P$	22, $2p^5 3s(^3P)3d\ ^4D$
$8^o_{1/2}$	6500 188.48	53, $2p^5 3s(^3P)3d\ ^4D$	23, $2p^5(3p^2\ ^3P)\ ^2P$	13, $2p^5 3s(^3P)3d\ ^2P$
$9^o_{1/2}$	6547 551.37	79, $2p^5(3p^2\ ^1S)\ ^2P$		
$10^o_{1/2}$	6560 344.42	24, $2p^5(3p^2\ ^3P)\ ^2P$	23, $2p^5(3p^2\ ^1D)\ ^2P$	23, $2p^5 3s(^1P)3d\ ^2P$
		12, $2p^5(3p^2\ ^1S)\ ^2P$		
$11^o_{1/2}$	6629 844.75	63, $2p^5 3s(^3P)3d\ ^2P$	21, $2p^5 3s(^1P)3d\ ^2P$	
$12^o_{1/2}$	7086 001.87	93, $2p^5(3d^2\ ^3F)\ ^4D$		
$13^o_{1/2}$	7143 845.04	37, $2p^5(3d^2\ ^3P)\ ^4P$	35, $2p^5(3d^2\ ^1D)\ ^2P$	14, $2p^5(3d^2\ ^3P)\ ^2P$
$14^o_{1/2}$	7155 468.37	37, $2p^5(3d^2\ ^3P)\ ^4P$	37, $2p^5(3d^2\ ^1D)\ ^2P$	17, $2p^5(3d^2\ ^3P)\ ^2S$
$15^o_{1/2}$	7215 108.75	49, $2p^5(3d^2\ ^3P)\ ^4D$	16, $2p^5(3d^2\ ^3P)\ ^2S$	16, $2p^5(3d^2\ ^1D)\ ^2P$
		15, $2p^5(3d^2\ ^3P)\ ^2P$		
$16^o_{1/2}$	7250 448.25	52, $2p^5(3d^2\ ^3P)\ ^2S$	23, $2p^5(3d^2\ ^3P)\ ^4D$	22, $2p^5(3d^2\ ^3P)\ ^4P$
$17^o_{1/2}$	7289 757.84	57, $2p^5(3d^2\ ^3P)\ ^2P$	17, $2p^5(3d^2\ ^3P)\ ^4D$	10, $2p^5(3d^2\ ^1D)\ ^2P$
$18^o_{1/2}$	7355 951.26	91, $2p^5(3d^2\ ^1S)\ ^2P$		
$1^o_{3/2}$	5798 374.25	97, $2p^5 3s^2\ ^2P$		
$2^o_{3/2}$	6311 725.79	39, $2p^5(3p^2\ ^3P)\ ^4P$	19, $2p^5(3p^2\ ^1D)\ ^2P$	14, $2p^5(3p^2\ ^3P)\ ^2P$
		11, $2p^5(3p^2\ ^3P)\ ^4D$		
$3^o_{3/2}$	6331 877.23	23, $2p^5(3p^2\ ^3P)\ ^4P$	22, $2p^5(3p^2\ ^1D)\ ^2P$	15, $2p^5(3p^2\ ^3P)\ ^4S$
		13, $2p^5(3p^2\ ^1D)\ ^2D$		
$4^o_{3/2}$	6349 533.49	60, $2p^5(3p^2\ ^3P)\ ^2D$	19, $2p^5(3p^2\ ^3P)\ ^4D$	11, $2p^5(3p^2\ ^3P)\ ^4P$
$5^o_{3/2}$	6408 720.63	38, $2p^5(3p^2\ ^3P)\ ^4S$	22, $2p^5(3p^2\ ^1D)\ ^2D$	10, $2p^5(3p^2\ ^3P)\ ^2D$
		9, $2p^5(3p^2\ ^3P)\ ^2P$		
$6^o_{3/2}$	6422 948.02	86, $2p^5 3s(^3P)3d\ ^4P$		
$7^o_{3/2}$	6427 301.06	44, $2p^5(3p^2\ ^3P)\ ^4D$	15, $2p^5(3p^2\ ^1D)\ ^2D$	12, $2p^5(3p^2\ ^3P)\ ^2D$
$8^o_{3/2}$	6446 426.41	48, $2p^5(3p^2\ ^1S)\ ^2P$	17, $2p^5(3p^2\ ^3P)\ ^4P$	17, $2p^5(3p^2\ ^3P)\ ^4S$
$9^o_{3/2}$	6457 919.22	19, $2p^5(3p^2\ ^1S)\ ^2P$	14, $2p^5(3p^2\ ^1D)\ ^2D$	11, $2p^5(3p^2\ ^3P)\ ^4S$
		9, $2p^5(3p^2\ ^1D)\ ^2P$		
$10^o_{3/2}$	6463 757.39	37, $2p^5 3s(^3P)3d\ ^4F$	27, $2p^5 3s(^1P)3d\ ^2D$	12, $2p^5 3s(^3P)3d\ ^4D$
$11^o_{3/2}$	6489 949.57	41, $2p^5 3s(^1P)3d\ ^2P$	24, $2p^5 3s(^3P)3d\ ^4D$	
$12^o_{3/2}$	6526 905.54	33, $2p^5 3s(^3P)3d\ ^4D$	18, $2p^5(3p^2\ ^3P)\ ^2P$	18, $2p^5 3s(^3P)3d\ ^2P$
$13^o_{3/2}$	6543 424.40	49, $2p^5 3s(^3P)3d\ ^4F$	31, $2p^5 3s(^1P)3d\ ^2D$	13, $2p^5 3s(^3P)3d\ ^2D$
$14^o_{3/2}$	6577 045.85	34, $2p^5(3p^2\ ^3P)\ ^2P$	21, $2p^5(3p^2\ ^1D)\ ^2P$	17, $2p^5 3s(^1P)3d\ ^2D$
		10, $2p^5 3s(^3P)3d\ ^2D$		
$15^o_{3/2}$	6599 042.88	31, $2p^5 3s(^1P)3d\ ^2P$	24, $2p^5 3s(^3P)3d\ ^2D$	20, $2p^5 3s(^3P)3d\ ^2P$
		10, $2p^5 3s(^3P)3d\ ^4D$		
$16^o_{3/2}$	6668 318.00	49, $2p^5 3s(^3P)3d\ ^2P$	15, $2p^5 3s(^3P)3d\ ^2D$	14, $2p^5(3p^2\ ^1D)\ ^2P$
		10, $2p^5 3s(^1P)3d\ ^2D$		
$17^o_{3/2}$	7088 331.50	83, $2p^5(3d^2\ ^3F)\ ^4D$		
$18^o_{3/2}$	7128 904.15	30, $2p^5(3d^2\ ^3F)\ ^4F$	25, $2p^5(3d^2\ ^1D)\ ^2D$	18, $2p^5(3d^2\ ^3F)\ ^2D$
		14, $2p^5(3d^2\ ^1D)\ ^2P$		
$19^o_{3/2}$	7136 445.93	65, $2p^5(3d^2\ ^3P)\ ^4P$	13, $2p^5(3d^2\ ^3F)\ ^4F$	
$20^o_{3/2}$	7154 574.60	27, $2p^5(3d^2\ ^3F)\ ^4F$	21, $2p^5(3d^2\ ^1D)\ ^2P$	15, $2p^5(3d^2\ ^1D)\ ^2D$
		10, $2p^5(3d^2\ ^3P)\ ^4P$		
$21^o_{3/2}$	7180 867.40	61, $2p^5(3d^2\ ^3P)\ ^2D$	20, $2p^5(3d^2\ ^3P)\ ^4D$	
$22^o_{3/2}$	7199 579.44	29, $2p^5(3d^2\ ^3P)\ ^4S$	25, $2p^5(3d^2\ ^1D)\ ^2D$	21, $2p^5(3d^2\ ^3P)\ ^2P$
$23^o_{3/2}$	7232 577.26	19, $2p^5(3d^2\ ^3P)\ ^4D$	19, $2p^5(3d^2\ ^3P)\ ^4S$	17, $2p^5(3d^2\ ^1D)\ ^2P$
		15, $2p^5(3d^2\ ^1S)\ ^2P$	12, $2p^5(3d^2\ ^3F)\ ^2D$	
$24^o_{3/2}$	7250 659.74	29, $2p^5(3d^2\ ^3P)\ ^4D$	27, $2p^5(3d^2\ ^3P)\ ^4S$	15, $2p^5(3d^2\ ^3P)\ ^4P$
		12, $2p^5(3d^2\ ^3P)\ ^2D$	11, $2p^5(3d^2\ ^1S)\ ^2P$	
$25^o_{3/2}$	7265 182.81	54, $2p^5(3d^2\ ^1S)\ ^2P$	23, $2p^5(3d^2\ ^1D)\ ^2P$	
$26^o_{3/2}$	7311 405.96	49, $2p^5(3d^2\ ^3F)\ ^2D$	18, $2p^5(3d^2\ ^1D)\ ^2D$	10, $2p^5(3d^2\ ^3P)\ ^2P$
$27^o_{3/2}$	7321 430.69	52, $2p^5(3d^2\ ^3P)\ ^2P$	18, $2p^5(3d^2\ ^1D)\ ^2P$	

Table 3. Energy level indices, their values (in cm^{-1}) relative to 1^e_0 level and configuration contributions of the Fe XV ion levels with $J = 1$.

Level index	Energy (cm^{-1})	Contributions (in per cent)		
1^e_0	0.00	97, $2p^6 3s^2\ ^1S$		
1^o_1	6147 739.62	58, $2p^5 3s(^3P)(3p^2\ ^3P)\ ^5P$	14, $2p^5 3s(^3P)(3p^2\ ^3P)\ ^5D$	7, $2p^5 3s(^1P)(3p^2\ ^3P)\ ^3P$
2^o_1	6174 676.75	44, $2p^5 3s(^1P)(3p^2\ ^3P)\ ^3D$ 9, $2p^5 3s(^3P)(3p^2\ ^3P)\ ^5P$	23, $2p^5 3s(^3P)(3p^2\ ^3P)\ ^3D$	18, $2p^5 3s(^3P)(3p^2\ ^3P)\ ^5D$
3^o_1	6191 267.43	30, $2p^5 3s(^3P)(3p^2\ ^1D)\ ^3P$ 9, $2p^5 3s(^3P)(3p^2\ ^3P)\ ^3P$	19, $2p^5 3s(^1P)(3p^2\ ^3P)\ ^3P$ 7, $2p^5 3s(^1P)(3p^2\ ^3P)\ ^3S$	11, $2p^5 3s(^3P)(3p^2\ ^3P)\ ^5P$
4^o_1	6231 893.67	40, $2p^5 3s(^3P)(3p^2\ ^3P)\ ^5D$ 7, $2p^5 3s(^1P)(3p^2\ ^1D)\ ^1P$	19, $2p^5 3s(^3P)(3p^2\ ^1D)\ ^3P$	10, $2p^5 3s(^1P)(3p^2\ ^3P)\ ^3D$
5^o_1	6246 529.03	43, $2p^5 3s(^1P)(3p^2\ ^1D)\ ^1P$ 8, $2p^5 3s(^3P)(3p^2\ ^3P)\ ^5D$	24, $2p^5 3s(^3P)(3p^2\ ^1D)\ ^3D$	10, $2p^5 3s(^3P)(3p^2\ ^3P)\ ^1P$
6^o_1	6258 293.40	32, $2p^5 3s(^1P)(3p^2\ ^3P)\ ^3S$ 12, $2p^5 3s(^3P)(3p^2\ ^3P)\ ^5D$	28, $2p^5 3s(^3P)(3p^2\ ^3P)\ ^3S$	17, $2p^5 3s(^3P)(3p^2\ ^3P)\ ^5P$
7^o_1	6288 597.95	39, $2p^5 3s(^1P)(3p^2\ ^3P)\ ^3P$ 9, $2p^5 3s(^1P)(3p^2\ ^1S)\ ^1P$	15, $2p^5 3s(^3P)(3p^2\ ^1D)\ ^3D$	10, $2p^5 3s(^1P)(3p^2\ ^3P)\ ^3S$
8^o_1	6329 178.78	20, $2p^5 3s(^3P)(3p^2\ ^1S)\ ^3P$ 10, $2p^5 3s(^3P)(3p^2\ ^3P)\ ^3P$	20, $2p^5 3s(^1P)(3p^2\ ^1S)\ ^1P$ 9, $2p^5 3s(^3P)(3p^2\ ^1D)\ ^3D$	17, $2p^5 3s(^1P)(3p^2\ ^3P)\ ^3P$
9^o_1	6337 249.68	21, $2p^5 3s(^1P)(3p^2\ ^1S)\ ^1P$ 16, $2p^5 3s(^3P)(3p^2\ ^1S)\ ^3P$	17, $2p^5 3s(^1P)(3p^2\ ^1D)\ ^1P$ 8, $2p^5 3s(^3P)(3p^2\ ^3P)\ ^3P$	16, $2p^5 3s(^3P)(3p^2\ ^1D)\ ^3D$ 7, $2p^5 3s(^3P)(3p^2\ ^3P)\ ^3S$
10^o_1	6350 857.59	36, $2p^5 3s^2 3d\ ^3P$	22, $2p^5 3s(^3P)(3p^2\ ^3P)\ ^3P$	12, $2p^5 3s(^3P)(3p^2\ ^1D)\ ^3D$
11^o_1	6387 516.45	29, $2p^5 3s(^3P)(3p^2\ ^3P)\ ^3D$ 10, $2p^5 3s(^1P)(3p^2\ ^3P)\ ^3S$	14, $2p^5 3s(^1P)(3p^2\ ^3P)\ ^3D$ 7, $2p^5 3s(^3P)(3p^2\ ^1S)\ ^3P$	11, $2p^5 3s(^3P)(3p^2\ ^3P)\ ^3S$ 7, $2p^5 3s^2 3d\ ^3P$
12^o_1	6406 899.00	29, $2p^5 3s^2 3d\ ^3P$ 10, $2p^5 3s^2 3d\ ^3D$	23, $2p^5 3s(^3P)(3p^2\ ^1D)\ ^3P$ 8, $2p^5 3s(^1P)(3p^2\ ^3P)\ ^3S$	15, $2p^5 3s(^3P)(3p^2\ ^3P)\ ^3S$ 7, $2p^5 3s(^1P)(3p^2\ ^3P)\ ^3P$
13^o_1	6421 423.44	44, $2p^5 3s(^3P)(3p^2\ ^1S)\ ^3P$	37, $2p^5 3s(^1P)(3p^2\ ^1S)\ ^1P$	9, $2p^5 3s(^3P)(3p^2\ ^3P)\ ^3D$
14^o_1	6435 776.92	31, $2p^5 3s(^3P)(3p^2\ ^3P)\ ^3P$ 9, $2p^5 3s(^1P)(3p^2\ ^3P)\ ^3D$	17, $2p^5 3s(^3P)(3p^2\ ^3P)\ ^3D$ 8, $2p^5 3s(^1P)(3p^2\ ^3P)\ ^3S$	10, $2p^5 3s(^3P)(3p^2\ ^3P)\ ^3S$
15^o_1	6459 950.72	54, $2p^5 3s^2 3d\ ^3D$	21, $2p^5 3s^2 3d\ ^1P$	9, $2p^5 3s(^3P)(3p^2\ ^1D)\ ^3D$
16^o_1	6504 115.15	63, $2p^5 3s(^3P)(3p^2\ ^3P)\ ^1P$	7, $2p^5 3s(^1P)(3p^2\ ^1D)\ ^1P$	
17^o_1	6566 910.79	63, $2p^5 3s^2 3d\ ^1P$	14, $2p^5 3s^2 3d\ ^3D$	9, $2p^5 3s(^1P)(3p^2\ ^1D)\ ^1P$
18^o_1	6840 706.65	59, $2p^5(3p^2\ ^3P)(^4P)3d\ ^5D$	19, $2p^5(3p^2\ ^3P)(^4D)3d\ ^5D$	15, $2p^5(3p^2\ ^3P)(^4S)3d\ ^5D$
19^o_1	6844 631.26	33, $2p^5(3p^2\ ^1D)(^2P)3d\ ^3P$ 9, $2p^5(3p^2\ ^3P)(^4P)3d\ ^3D$	15, $2p^5(3p^2\ ^3P)(^2P)3d\ ^3D$	12, $2p^5(3p^2\ ^1D)(^2D)3d\ ^3D$
20^o_1	6862 886.91	59, $2p^5(3p^2\ ^3P)(^4P)3d\ ^5P$	34, $2p^5(3p^2\ ^3P)(^4D)3d\ ^5P$	
21^o_1	6889 714.99	69, $2p^5(3p^2\ ^3P)(^4P)3d\ ^5F$		
22^o_1	6901 127.27	15, $2p^5(3p^2\ ^3P)(^4D)3d\ ^3P$ 7, $2p^5(3p^2\ ^1D)(^2F)3d\ ^3P$	8, $2p^5(3p^2\ ^3P)(^2D)3d\ ^3P$	8, $2p^5(3p^2\ ^1D)(^2P)3d\ ^1P$
23^o_1	6902 205.00	22, $2p^5(3p^2\ ^3P)(^4D)3d\ ^3S$ 9, $2p^5(3p^2\ ^1D)(^2D)3d\ ^1P$	18, $2p^5(3p^2\ ^3P)(^2D)3d\ ^3S$ 9, $2p^5(3p^2\ ^1S)(^2P)3d\ ^3D$	17, $2p^5(3p^2\ ^3P)(^2D)3d\ ^1P$
24^o_1	6927 478.71	42, $2p^5(3p^2\ ^3P)(^4D)3d\ ^5F$	29, $2p^5(3p^2\ ^3P)(^2D)3d\ ^3D$	
25^o_1	6941 493.09	16, $2p^5(3p^2\ ^3P)(^4S)3d\ ^5D$ 11, $2p^5(3p^2\ ^1D)(^2F)3d\ ^3P$	15, $2p^5(3p^2\ ^1D)(^2P)3d\ ^1P$ 11, $2p^5(3p^2\ ^1D)(^2D)3d\ ^3S$	13, $2p^5(3p^2\ ^3P)(^2P)3d\ ^3P$
26^o_1	6945 122.56	10, $2p^5(3p^2\ ^1D)(^2D)3d\ ^3D$	9, $2p^5(3p^2\ ^1S)(^2P)3d\ ^3D$	7, $2p^5(3p^2\ ^3P)(^2D)3d\ ^3S$
27^o_1	6959 918.90	19, $2p^5(3p^2\ ^3P)(^2D)3d\ ^3P$	18, $2p^5(3p^2\ ^3P)(^4D)3d\ ^5D$	9, $2p^5(3p^2\ ^3P)(^4P)3d\ ^5D$
28^o_1	6967 028.92	13, $2p^5(3p^2\ ^1D)(^2F)3d\ ^3P$ 8, $2p^5(3p^2\ ^3P)(^4P)3d\ ^5P$	11, $2p^5(3p^2\ ^3P)(^4D)3d\ ^5P$ 8, $2p^5(3p^2\ ^3P)(^2D)3d\ ^1P$	10, $2p^5(3p^2\ ^3P)(^2D)3d\ ^3S$ 7, $2p^5(3p^2\ ^3P)(^4D)3d\ ^3D$
29^o_1	6974 896.38	28, $2p^5(3p^2\ ^3P)(^2S)3d\ ^3D$ 7, $2p^5(3p^2\ ^3P)(^4P)3d\ ^3P$	17, $2p^5(3p^2\ ^3P)(^2D)3d\ ^3D$	8, $2p^5(3p^2\ ^3P)(^4P)3d\ ^3D$
30^o_1	6979 899.50	22, $2p^5(3p^2\ ^1S)(^2P)3d\ ^1P$ 8, $2p^5(3p^2\ ^3P)(^4P)3d\ ^3D$ 7, $2p^5(3p^2\ ^1D)(^2P)3d\ ^1P$	14, $2p^5(3p^2\ ^3P)(^4S)3d\ ^5D$ 8, $2p^5(3p^2\ ^3P)(^4P)3d\ ^3P$	12, $2p^5(3p^2\ ^3P)(^4D)3d\ ^5D$ 7, $2p^5(3p^2\ ^3P)(^2D)3d\ ^3D$
31^o_1	6988 099.03	22, $2p^5(3p^2\ ^3P)(^2S)3d\ ^3D$ 9, $2p^5(3p^2\ ^3P)(^4P)3d\ ^5F$	14, $2p^5(3p^2\ ^3P)(^4D)3d\ ^5F$ 8, $2p^5(3p^2\ ^3P)(^4P)3d\ ^3D$	11, $2p^5(3p^2\ ^3P)(^4D)3d\ ^3D$
32^o_1	6993 174.84	15, $2p^5(3p^2\ ^3P)(^4S)3d\ ^5D$ 7, $2p^5(3p^2\ ^3P)(^2D)3d\ ^3P$	11, $2p^5(3p^2\ ^1S)(^2P)3d\ ^3D$ 7, $2p^5(3p^2\ ^3P)(^2S)3d\ ^3D$	7, $2p^5(3p^2\ ^3P)(^4D)3d\ ^3P$
33^o_1	6996 219.63	18, $2p^5(3p^2\ ^3P)(^4D)3d\ ^5P$ 8, $2p^5(3p^2\ ^3P)(^4D)3d\ ^3P$	11, $2p^5(3p^2\ ^3P)(^4P)3d\ ^5P$ 7, $2p^5(3p^2\ ^1D)(^2F)3d\ ^3P$	9, $2p^5(3p^2\ ^3P)(^4D)3d\ ^3S$ 7, $2p^5(3p^2\ ^1D)(^2P)3d\ ^1P$
34^o_1	6999 955.71	88, $2p^5 3s(^3P)(3d^2\ ^3F)\ ^3D$		
35^o_1	7009 064.96	10, $2p^5(3p^2\ ^3P)(^4P)3d\ ^3D$ 7, $2p^5(3p^2\ ^3P)(^4D)3d\ ^5F$	10, $2p^5(3p^2\ ^3P)(^2S)3d\ ^3D$ 7, $2p^5(3p^2\ ^1D)(^2D)3d\ ^1P$	8, $2p^5(3p^2\ ^1D)(^2D)3d\ ^3D$
36^o_1	7015 007.38	11, $2p^5(3p^2\ ^3P)(^4S)3d\ ^5D$ 7, $2p^5(3p^2\ ^1D)(^2F)3d\ ^3D$	11, $2p^5(3p^2\ ^1D)(^2P)3d\ ^3D$ 7, $2p^5(3p^2\ ^1S)(^2P)3d\ ^1P$	8, $2p^5(3p^2\ ^3P)(^2D)3d\ ^1P$

Table 3 – *continued*

Level index	Energy (cm^{-1})	Contributions (in per cent)		
37^o_1	7018 904.13	24, $2p^5(3p^2\ ^3P)(^2D)3d\ ^1P$	16, $2p^5(3p^2\ ^1D)(^2D)3d\ ^1P$	9, $2p^5(3p^2\ ^3P)(^4S)3d\ ^3D$
		7, $2p^5(3p^2\ ^3P)(^4D)3d\ ^3P$	7, $2p^5(3p^2\ ^3P)(^2D)3d\ ^3D$	
38^o_1	7038 548.12	14, $2p^5(3p^2\ ^3P)(^2D)3d\ ^3P$	14, $2p^53s(^3P)(3d^2\ ^3P)\ ^5D$	12, $2p^53s(^3P)(3d^2\ ^3F)\ ^5D$
		8, $2p^5(3p^2\ ^1S)(^2P)3d\ ^1P$	7, $2p^5(3p^2\ ^3P)(^2P)3d\ ^3D$	
39^o_1	7040 724.02	13, $2p^5(3p^2\ ^1D)(^2F)3d\ ^1P$	12, $2p^5(3p^2\ ^1D)(^2D)3d\ ^3S$	7, $2p^5(3p^2\ ^1D)(^2D)3d\ ^1P$
40^o_1	7046 813.82	49, $2p^53s(^3P)(3d^2\ ^3F)\ ^5D$	9, $2p^53s(^3P)(3d^2\ ^3P)\ ^5D$	
41^o_1	7050 112.33	19, $2p^5(3p^2\ ^3P)(^4P)3d\ ^3D$	8, $2p^5(3p^2\ ^3P)(^2P)3d\ ^3D$	7, $2p^5(3p^2\ ^3P)(^4S)3d\ ^3D$
42^o_1	7059 660.35	71, $2p^53s(^3P)(3d^2\ ^3P)\ ^3D$	7, $2p^53s(^1P)(3d^2\ ^3P)\ ^3S$	
43^o_1	7064 022.85	13, $2p^5(3p^2\ ^3P)(^4S)3d\ ^3D$	10, $2p^5(3p^2\ ^3P)(^4P)3d\ ^3P$	8, $2p^53s(^3P)(3d^2\ ^3F)\ ^5D$
		8, $2p^53s(^1P)(3d^2\ ^3F)\ ^3D$		
44^o_1	7069 206.33	20, $2p^5(3p^2\ ^1S)(^2P)3d\ ^3P$	8, $2p^5(3p^2\ ^3P)(^4D)3d\ ^3D$	8, $2p^5(3p^2\ ^3P)(^4S)3d\ ^3D$
		7, $2p^53s(^3P)(3d^2\ ^3F)\ ^5D$		
45^o_1	7081 975.89	18, $2p^5(3p^2\ ^1D)(^2P)3d\ ^3D$	13, $2p^53s(^3P)(3d^2\ ^1D)\ ^3P$	12, $2p^5(3p^2\ ^3P)(^2P)3d\ ^3P$
		7, $2p^53s(^1P)(3d^2\ ^3P)\ ^3P$		
46^o_1	7088 323.63	12, $2p^5(3p^2\ ^3P)(^2D)3d\ ^3S$	9, $2p^5(3p^2\ ^1D)(^2F)3d\ ^3D$	7, $2p^53s(^3P)(3d^2\ ^1D)\ ^3P$
47^o_1	7096 320.01	18, $2p^5(3p^2\ ^3P)(^4D)3d\ ^3P$	10, $2p^5(3p^2\ ^3P)(^4D)3d\ ^3S$	7, $2p^5(3p^2\ ^3P)(^4P)3d\ ^3P$
		7, $2p^53s(^3P)(3d^2\ ^1D)\ ^3P$		
48^o_1	7097 641.29	16, $2p^53s(^1P)(3d^2\ ^3P)\ ^3D$	13, $2p^53s(^3P)(3d^2\ ^3P)\ ^5P$	10, $2p^5(3p^2\ ^1D)(^2P)3d\ ^3D$
		9, $2p^5(3p^2\ ^1D)(^2D)3d\ ^3S$		
49^o_1	7102 194.62	30, $2p^53s(^1P)(3d^2\ ^3P)\ ^3D$	10, $2p^5(3p^2\ ^3P)(^4D)3d\ ^3P$	8, $2p^53s(^1P)(3d^2\ ^3P)\ ^3P$
		7, $2p^5(3p^2\ ^1D)(^2D)3d\ ^3S$		
50^o_1	7108 998.97	15, $2p^5(3p^2\ ^3P)(^4D)3d\ ^3D$	15, $2p^5(3p^2\ ^3P)(^2P)3d\ ^3D$	7, $2p^5(3p^2\ ^3P)(^4D)3d\ ^3S$
51^o_1	7118 590.36	15, $2p^5(3p^2\ ^3P)(^4D)3d\ ^3S$	11, $2p^5(3p^2\ ^3P)(^2D)3d\ ^3S$	11, $2p^5(3p^2\ ^1S)(^2P)3d\ ^3P$
		8, $2p^5(3p^2\ ^3P)(^2D)3d\ ^3P$	7, $2p^5(3p^2\ ^3P)(^4D)3d\ ^3P$	
52^o_1	7121 107.39	21, $2p^53s(^1P)(3d^2\ ^1D)\ ^1P$	20, $2p^53s(^3P)(3d^2\ ^1D)\ ^3D$	8, $2p^5(3p^2\ ^1S)(^2P)3d\ ^3P$
		7, $2p^5(3p^2\ ^1D)(^2D)3d\ ^3D$	7, $2p^53s(^1P)(3d^2\ ^3F)\ ^3D$	
53^o_1	7134 194.37	17, $2p^53s(^3P)(3d^2\ ^1D)\ ^3P$	13, $2p^53s(^3P)(3d^2\ ^3P)\ ^5P$	8, $2p^5(3p^2\ ^1D)(^2D)3d\ ^3S$
		7, $2p^53s(^3P)(3d^2\ ^3P)\ ^3S$	7, $2p^53s(^1P)(3d^2\ ^1D)\ ^1P$	
54^o_1	7138 272.28	18, $2p^5(3p^2\ ^1D)(^2F)3d\ ^1P$	13, $2p^5(3p^2\ ^3P)(^2P)3d\ ^3P$	
55^o_1	7140 630.62	25, $2p^5(3p^2\ ^1D)(^2F)3d\ ^1P$	11, $2p^5(3p^2\ ^3P)(^2P)3d\ ^3P$	9, $2p^53s(^3P)(3d^2\ ^3P)\ ^1P$
		8, $2p^5(3p^2\ ^1D)(^2F)3d\ ^3P$		
56^o_1	7144 478.01	19, $2p^5(3p^2\ ^3P)(^4S)3d\ ^3D$	13, $2p^53s(^3P)(3d^2\ ^3F)\ ^5F$	8, $2p^5(3p^2\ ^3P)(^4D)3d\ ^3D$
57^o_1	7164 762.25	25, $2p^53s(^3P)(3d^2\ ^3P)\ ^5P$	11, $2p^53s(^1P)(3d^2\ ^3P)\ ^3S$	8, $2p^53s(^1P)(3d^2\ ^3F)\ ^3D$
58^o_1	7170 702.77	29, $2p^53s(^3P)(3d^2\ ^3P)\ ^5D$	22, $2p^5(3p^2\ ^1D)(^2P)3d\ ^3P$	16, $2p^5(3p^2\ ^3P)(^2P)3d\ ^3D$
		7, $2p^53s(^1P)(3d^2\ ^3P)\ ^3S$		
59^o_1	7171 829.48	14, $2p^53s(^3P)(3d^2\ ^3P)\ ^3S$	10, $2p^53s(^1P)(3d^2\ ^3P)\ ^3S$	9, $2p^53s(^3P)(3d^2\ ^3F)\ ^5F$
		8, $2p^53s(^3P)(3d^2\ ^3P)\ ^3D$		
60^o_1	7196 956.72	36, $2p^53s(^1P)(3d^2\ ^3P)\ ^3P$	17, $2p^53s(^1P)(3d^2\ ^3P)\ ^3S$	9, $2p^5(3p^2\ ^1D)(^2P)3d\ ^1P$
61^o_1	7208 809.42	44, $2p^53s(^3P)(3d^2\ ^3F)\ ^5F$	13, $2p^5(3p^2\ ^1S)(^2P)3d\ ^3P$	
62^o_1	7217 798.64	22, $2p^53s(^1P)(3d^2\ ^3F)\ ^3D$	20, $2p^53s(^1P)(3d^2\ ^1S)\ ^1P$	16, $2p^53s(^3P)(3d^2\ ^1S)\ ^3P$
		8, $2p^53s(^1P)(3d^2\ ^1D)\ ^1P$	7, $2p^53s(^3P)(3d^2\ ^3P)\ ^5D$	
63^o_1	7222 757.56	29, $2p^53s(^3P)(3d^2\ ^3P)\ ^3P$	9, $2p^53s(^3P)(3d^2\ ^1D)\ ^3P$	
64^o_1	7236 310.32	17, $2p^53s(^3P)(3d^2\ ^1S)\ ^3P$	12, $2p^5(3p^2\ ^3P)(^2P)3d\ ^1P$	11, $2p^53s(^1P)(3d^2\ ^1S)\ ^1P$
		9, $2p^53s(^1P)(3d^2\ ^3F)\ ^3D$		
65^o_1	7251 963.66	25, $2p^5(3p^2\ ^3P)(^2P)3d\ ^1P$	14, $2p^5(3p^2\ ^1S)(^2P)3d\ ^3D$	7, $2p^53s(^3P)(3d^2\ ^3P)\ ^3S$
		7, $2p^53s(^1P)(3d^2\ ^3P)\ ^3S$		
66^o_1	7261 771.50	19, $2p^53s(^1P)(3d^2\ ^1D)\ ^1P$	16, $2p^53s(^3P)(3d^2\ ^1D)\ ^3D$	8, $2p^53s(^1P)(3d^2\ ^3F)\ ^3D$
		8, $2p^53s(^3P)(3d^2\ ^3P)\ ^3S$		
67^o_1	7297 507.81	12, $2p^53s(^1P)(3d^2\ ^3P)\ ^3D$	9, $2p^53s(^3P)(3d^2\ ^3P)\ ^3P$	7, $2p^5(3p^2\ ^1D)(^2D)3d\ ^3D$
68^o_1	7311 658.30	40, $2p^53s(^3P)(3d^2\ ^1S)\ ^3P$	31, $2p^53s(^1P)(3d^2\ ^1S)\ ^1P$	
69^o_1	7344 267.16	42, $2p^53s(^3P)(3d^2\ ^3P)\ ^1P$	11, $2p^5(3p^2\ ^1D)(^2F)3d\ ^1P$	
70^o_1	7714 655.12	72, $2p^5(3d^3\ ^4F)\ ^5D$	19, $2p^5(3d^3\ ^4F)\ ^5F$	8, $2p^5(3d^3\ ^4P)\ ^5D$
71^o_1	7733 634.82	58, $2p^5(3d^3\ ^4F)\ ^5F$	16, $2p^5(3d^3\ ^4F)\ ^3D$	13, $2p^5(3d^3\ ^4F)\ ^5D$
72^o_1	7770 067.00	28, $2p^5(3d^3\ ^2P)\ ^3P$	27, $2p^5(3d^3\ {}^2_3D)\ ^3P$	11, $2p^5(3d^3\ ^2P)\ ^3S$
		9, $2p^5(3d^3\ {}^2_3D)\ ^3D$	8, $2p^5(3d^3\ {}^2_1D)\ ^3P$	
73^o_1	7782 871.89	16, $2p^5(3d^3\ ^4P)\ ^5D$	14, $2p^5(3d^3\ {}^2_3D)\ ^3D$	13, $2p^5(3d^3\ {}^2_3D)\ ^1P$
		11, $2p^5(3d^3\ ^4P)\ ^3D$	8, $2p^5(3d^3\ ^4P)\ ^3P$	
74^o_1	7784 674.79	17, $2p^5(3d^3\ ^4P)\ ^5P$	15, $2p^5(3d^3\ ^4P)\ ^3P$	11, $2p^5(3d^3\ {}^2_3D)\ ^3D$
		11, $2p^5(3d^3\ ^2P)\ ^3P$	10, $2p^5(3d^3\ ^2P)\ ^3S$	8, $2p^5(3d^3\ {}^2_3D)\ ^3P$
75^o_1	7794 765.11	37, $2p^5(3d^3\ ^4P)\ ^3D$	32, $2p^5(3d^3\ ^2F)\ ^3D$	
76^o_1	7806 306.82	17, $2p^5(3d^3\ ^2P)\ ^3S$	16, $2p^5(3d^3\ ^4P)\ ^3S$	15, $2p^5(3d^3\ ^4P)\ ^3P$
		11, $2p^5(3d^3\ ^4P)\ ^5D$	10, $2p^5(3d^3\ ^2P)\ ^1P$	

Table 3 – *continued*

Level index	Energy (cm^{-1})	Contributions (in per cent)		
77^o_1	7823 526.67	34, $2p^5(3d^3\ ^4P)\ ^5P$	16, $2p^5(3d^3\ ^2P)\ ^3P$	13, $2p^5(3d^3\ ^2_3D)\ ^3P$
		13, $2p^5(3d^3\ ^2_3D)\ ^1P$		
78^o_1	7841 169.07	39, $2p^5(3d^3\ ^2_1D)\ ^3P$	13, $2p^5(3d^3\ ^2F)\ ^3D$	10, $2p^5(3d^3\ ^4P)\ ^3D$
		7, $2p^5(3d^3\ ^4P)\ ^3P$		
79^o_1	7851 139.10	20, $2p^5(3d^3\ ^4P)\ ^5D$	19, $2p^5(3d^3\ ^2P)\ ^3D$	17, $2p^5(3d^3\ ^4P)\ ^5P$
		8, $2p^5(3d^3\ ^2_3D)\ ^3D$	7, $2p^5(3d^3\ ^2P)\ ^3S$	
80^o_1	7860 735.41	18, $2p^5(3d^3\ ^2_3D)\ ^1P$	16, $2p^5(3d^3\ ^4P)\ ^5D$	15, $2p^5(3d^3\ ^2P)\ ^3D$
		11, $2p^5(3d^3\ ^4F)\ ^3D$	10, $2p^5(3d^3\ ^2_3D)\ ^3P$	
81^o_1	7874 067.28	26, $2p^5(3d^3\ ^2_1D)\ ^3P$	18, $2p^5(3d^3\ ^2F)\ ^3D$	13, $2p^5(3d^3\ ^2P)\ ^3P$
		8, $2p^5(3d^3\ ^4F)\ ^3D$	7, $2p^5(3d^3\ ^4P)\ ^3D$	7, $2p^5(3d^3\ ^2P)\ ^3D$
82^o_1	7888 117.15	15, $2p^5(3d^3\ ^2P)\ ^3P$	10, $2p^5(3d^3\ ^2F)\ ^3D$	10, $2p^5(3d^3\ ^2_3D)\ ^3D$
		10, $2p^5(3d^3\ ^2P)\ ^3S$	10, $2p^5(3d^3\ ^2_1D)\ ^3D$	9, $2p^5(3d^3\ ^4P)\ ^3D$
		7, $2p^5(3d^3\ ^4P)\ ^5P$	7, $2p^5(3d^3\ ^2P)\ ^3D$	
83^o_1	7902 900.41	32, $2p^5(3d^3\ ^4P)\ ^3P$	15, $2p^5(3d^3\ ^2_3D)\ ^3P$	9, $2p^5(3d^3\ ^4P)\ ^5D$
		9, $2p^5(3d^3\ ^2_1D)\ ^3P$	7, $2p^5(3d^3\ ^4F)\ ^3D$	
84^o_1	7928 082.97	38, $2p^5(3d^3\ ^2_1D)\ ^3D$	18, $2p^5(3d^3\ ^2_1D)\ ^1P$	11, $2p^5(3d^3\ ^2P)\ ^1P$
		7, $2p^5(3d^3\ ^4F)\ ^3D$		
85^o_1	7943 443.25	36, $2p^5(3d^3\ ^4F)\ ^3D$	26, $2p^5(3d^3\ ^2P)\ ^3D$	12, $2p^5(3d^3\ ^2_3D)\ ^3D$
86^o_1	7957 251.08	40, $2p^5(3d^3\ ^4P)\ ^3S$	12, $2p^5(3d^3\ ^2P)\ ^3S$	8, $2p^5(3d^3\ ^2_3D)\ ^3D$
		8, $2p^5(3d^3\ ^2_3D)\ ^1P$	7, $2p^5(3d^3\ ^4P)\ ^3P$	
87^o_1	7971 441.35	38, $2p^5(3d^3\ ^2P)\ ^1P$	21, $2p^5(3d^3\ ^2_3D)\ ^1P$	12, $2p^5(3d^3\ ^2P)\ ^3S$
		9, $2p^5(3d^3\ ^4P)\ ^3S$		
88^o_1	8015 934.65	65, $2p^5(3d^3\ ^2_1D)\ ^1P$	24, $2p^5(3d^3\ ^2_1D)\ ^3D$	

where $g_j = 2J_j + 1$ is the statistical weight of the excited-state level.

We present the electric-dipole transition array 2p–3*l* wavelengths λ_{ij} and the absorption oscillator strengths f_{ij} from the ground-state $2p^63s\ ^2S_{1/2}$ level to the individual levels of the upper state of Fe XVI in Table 4. In addition, we provide the associated emission transition probabilities A_{ji} from the excited $2p^53l3l'$ configuration fine-structure levels $J = 1/2$ and $3/2$ to the ground state in the same table. The electric dipole transition probabilities presented here were calculated in the length form. Results sorted for the transition arrays between different total J values and listed in ascending wavelength.

The 2p–3*l* transition atomic data for Fe XV are presented in Table 5. In this case the selection rules allow only the transitions from the ground level $2p^63s^2\ ^1S_0$ to the fine-structure levels with $J = 1$ of the upper state having a vacancy in the 2p shell. The absorption oscillator strengths f_{ij} and emission transition probabilities A_{ji} were calculated in both the length and velocity form, although we choose to present only the data obtained in the length form. Data are once again presented in ascending wavelength.

4 DISCUSSION

To the best of our knowledge, there are no publicly available detailed atomic data (either theoretical or experimental) for electric dipole transitions involving the inner-shell 2p electrons in Fe XV and Fe XVI. The situation is similar for the lower ionization stages of iron ions.

In this context, the work of Behar et al. (2001) should be mentioned, where the calculation of atomic data and their use for the modelling of Fe^{0+}–Fe^{15+} absorption spectra was reported. As a result of the need to obtain large quantities of atomic data, and for the sake of simplifying the computations, the approximation used in their work was very limited in choosing the CI wavefunction expansion. When considering 2p excited states, the configuration mixing was restricted to $2s^22p^5[3s3d + 3p^2]$ in the case of Fe XVI and to $2s^22p^5[3s^23d + 3s3p^2]$ for Fe XV. Unfortunately, we cannot make a comparison of our atomic data with those of Behar et al. (2001), because detailed results on electric dipole transitions (line wavelengths, oscillator strengths) were not presented in their paper. Instead, we examine internal indicators of the accuracy of our calculated atomic data, as discussed by Hibbert (1996).

One of the possible ways to evaluate the accuracy of the calculated E1-transition atomic data is to compare f-values estimated using the length form (equation 6) against those obtained using the velocity form (equation 7). Good agreement would provide support for the accuracy of the wavefunctions used in the calculation, and indicate that they should lead to reliable atomic data. A traditional way to do this is to plot $\log(f_V)$ against $\log(f_L)$.

In Fig. 1 the velocity-form oscillator strengths $\log(f_V)$ are plotted against the length-form oscillator strengths $\log(f_L)$ for all lines from the 2p–3*l* transition array in Fe XVI. We present a comparison for the three different wavefunction expansions. The first set of data (*set 1*) was calculated using a truncated CI wavefunction expansion consisting only of the configurations with $n = 3$ electrons from the configuration set described in Section 2.2. The next set of data (*set 2*) was calculated by adding configurations having one $n = 4$ electron, whereas the last set (*set 3*) was calculated with the wavefunction expansion including all configurations listed in Section 2.2.

One can see from Fig. 1 that there is good agreement between the length- and velocity-form transition data in general, and that the best agreement is achieved including all described configurations in the wavefunction expansion. In this case agreement is within 10 per cent, with the exception of a few transitions that have oscillator strengths $f_{if} < 5 \times 10^{-5}$. These lines represent transitions to the levels of the $2p^53d^2$ configurations, which would be forbidden in non-relativistic *LS*-coupling.

Table 4. Electric dipole transition 2p–3*l* wavelengths λ (in Å), absorption oscillator strengths f_{ij} (in au) and corresponding emission transition probabilities A_{ji} (in s^{-1}) for the Fe XVI ions.

Level index lower	upper	λ (Å)	f_{ij}	A_{ji} (s^{-1})
			1/2–1/2	
$1^e_{1/2}$	$18^o_{1/2}$	13.594 43	1.987 (−5)	7.173 (+8)
$1^e_{1/2}$	$17^o_{1/2}$	13.717 88	5.537 (−4)	1.963 (+10)
$1^e_{1/2}$	$16^o_{1/2}$	13.792 25	7.443 (−6)	2.610 (+8)
$1^e_{1/2}$	$15^o_{1/2}$	13.859 80	5.289 (−4)	1.837 (+10)
$1^e_{1/2}$	$14^o_{1/2}$	13.975 32	4.119 (−4)	1.407 (+10)
$1^e_{1/2}$	$13^o_{1/2}$	13.998 06	3.010 (−4)	1.025 (+10)
$1^e_{1/2}$	$12^o_{1/2}$	14.112 33	3.466 (−8)	1.161 (+6)
$1^e_{1/2}$	$11^o_{1/2}$	15.083 31	7.956 (−1)	2.333 (+13)
$1^e_{1/2}$	$10^o_{1/2}$	15.243 10	4.390 (−4)	1.260 (+10)
$1^e_{1/2}$	$9^o_{1/2}$	15.272 88	7.625 (−4)	2.180 (+10)
$1^e_{1/2}$	$8^o_{1/2}$	15.384 17	1.129 (−1)	3.183 (+12)
$1^e_{1/2}$	$7^o_{1/2}$	15.457 84	1.275 (−2)	3.560 (+11)
$1^e_{1/2}$	$6^o_{1/2}$	15.539 61	2.693 (−6)	7.440 (+7)
$1^e_{1/2}$	$5^o_{1/2}$	15.586 91	1.261 (−3)	3.463 (+10)
$1^e_{1/2}$	$4^o_{1/2}$	15.626 60	1.592 (−3)	4.348 (+10)
$1^e_{1/2}$	$3^o_{1/2}$	15.748 02	3.106 (−3)	8.353 (+10)
$1^e_{1/2}$	$2^o_{1/2}$	15.837 34	9.166 (−3)	2.438 (+11)
$1^e_{1/2}$	$1^o_{1/2}$	16.965 14	3.091 (−2)	7.163 (+11)
			1/2–1/3	
$1^e_{1/2}$	$27^o_{3/2}$	13.658 53	1.454 (−3)	2.599 (+10)
$1^e_{1/2}$	$26^o_{3/2}$	13.677 26	4.204 (−7)	7.495 (+6)
$1^e_{1/2}$	$25^o_{3/2}$	13.764 28	5.341 (−4)	9.402 (+9)
$1^e_{1/2}$	$24^o_{3/2}$	13.791 85	1.127 (−9)	1.977 (+4)
$1^e_{1/2}$	$23^o_{3/2}$	13.826 33	5.497 (−4)	9.590 (+9)
$1^e_{1/2}$	$22^o_{3/2}$	13.889 70	3.987 (−5)	6.892 (+8)
$1^e_{1/2}$	$21^o_{3/2}$	13.925 89	4.573 (−5)	7.864 (+8)
$1^e_{1/2}$	$20^o_{3/2}$	13.977 07	3.999 (−4)	6.827 (+9)
$1^e_{1/2}$	$19^o_{3/2}$	14.012 58	2.020 (−7)	3.430 (+6)
$1^e_{1/2}$	$18^o_{3/2}$	14.027 40	2.638 (−4)	4.472 (+9)
$1^e_{1/2}$	$17^o_{3/2}$	14.107 69	2.463 (−7)	4.127 (+6)
$1^e_{1/2}$	$16^o_{3/2}$	14.996 28	6.975 (−1)	1.034 (+13)
$1^e_{1/2}$	$15^o_{3/2}$	15.153 71	8.419 (−1)	1.223 (+13)
$1^e_{1/2}$	$14^o_{3/2}$	15.204 39	1.666 (−2)	2.403 (+11)
$1^e_{1/2}$	$13^o_{3/2}$	15.282 52	1.362 (−2)	1.945 (+11)
$1^e_{1/2}$	$12^o_{3/2}$	15.321 19	1.190 (−1)	1.691 (+12)
$1^e_{1/2}$	$11^o_{3/2}$	15.408 44	1.587 (−1)	2.230 (+12)
$1^e_{1/2}$	$10^o_{3/2}$	15.470 88	5.816 (−3)	8.104 (+10)
$1^e_{1/2}$	$9^o_{3/2}$	15.484 86	2.295 (−4)	3.192 (+9)
$1^e_{1/2}$	$8^o_{3/2}$	15.512 47	3.322 (−3)	4.605 (+10)
$1^e_{1/2}$	$7^o_{3/2}$	15.558 63	6.313 (−4)	8.698 (+9)
$1^e_{1/2}$	$6^o_{3/2}$	15.569 17	5.667 (−3)	7.797 (+10)
$1^e_{1/2}$	$5^o_{3/2}$	15.603 74	1.235 (−3)	1.691 (+10)
$1^e_{1/2}$	$4^o_{3/2}$	15.749 19	9.991 (−6)	1.343 (+8)
$1^e_{1/2}$	$3^o_{3/2}$	15.793 10	8.938 (−3)	1.195 (+11)
$1^e_{1/2}$	$2^o_{3/2}$	15.843 53	4.425 (−3)	5.880 (+10)
$1^e_{1/2}$	$1^o_{3/2}$	17.246 21	6.272 (−2)	7.033 (+11)

Another trend evident from Fig. 1 is that inclusion of the configurations with the $\bar{4}l$ correlation orbitals significantly changes some *f*-values (compare *set 1* and *set 2*). A more detailed analysis of data reveals that electric dipole transition oscillator strengths change by up to 30 per cent, even for stronger ($f_L > 10^{-2}$) lines. Consequently, it allows us to conclude that use of a limited CI wavefunction expansion with only $n = 3$ shell configurations included (as

Table 5. Electric dipole transition 2p–3*l* wavelengths λ (in Å), absorption oscillator strengths f_{ij} (in au) and corresponding emission transition probabilities A_{ji} (in s^{-1}) for the Fe XV ions.

Level index lower	upper	λ (Å)	f_{ij}	A_{ji} (s^{-1})
1^e_0	88^o_1	12.475 15	3.446 (−6)	4.923 (+7)
1^e_0	87^o_1	12.544 78	5.546 (−6)	7.836 (+7)
1^e_0	86^o_1	12.567 15	2.883 (−7)	4.058 (+6)
1^e_0	85^o_1	12.589 00	5.302 (−7)	7.438 (+6)
1^e_0	84^o_1	12.613 39	4.057 (−6)	5.670 (+7)
1^e_0	83^o_1	12.653 58	1.046 (−6)	1.453 (+7)
1^e_0	82^o_1	12.677 30	5.240 (−7)	7.249 (+6)
1^e_0	81^o_1	12.699 92	5.884 (−9)	8.111 (+4)
1^e_0	80^o_1	12.721 45	5.535 (−7)	7.604 (+6)
1^e_0	79^o_1	12.737 00	1.050 (−6)	1.439 (+7)
1^e_0	78^o_1	12.753 20	3.090 (−8)	4.225 (+5)
1^e_0	77^o_1	12.781 96	3.705 (−7)	5.043 (+6)
1^e_0	76^o_1	12.810 15	1.750 (−7)	2.371 (+6)
1^e_0	75^o_1	12.829 12	1.294 (−7)	1.749 (+6)
1^e_0	74^o_1	12.845 75	3.456 (−9)	4.657 (+4)
1^e_0	73^o_1	12.848 73	6.551 (−8)	8.823 (+5)
1^e_0	72^o_1	12.869 90	2.546 (−8)	3.418 (+5)
1^e_0	71^o_1	12.930 53	5.309 (−9)	7.059 (+4)
1^e_0	70^o_1	12.962 34	2.689 (−10)	3.558 (+3)
1^e_0	69^o_1	13.616 06	1.162 (−3)	1.394 (+10)
1^e_0	68^o_1	13.676 79	1.857 (−6)	2.207 (+7)
1^e_0	67^o_1	13.703 31	1.472 (−5)	1.743 (+8)
1^e_0	66^o_1	13.770 74	1.837 (−3)	2.154 (+10)
1^e_0	65^o_1	13.789 37	3.250 (−7)	3.801 (+6)
1^e_0	64^o_1	13.819 20	4.788 (−6)	5.574 (+7)
1^e_0	63^o_1	13.845 13	2.414 (−4)	2.800 (+9)
1^e_0	62^o_1	13.854 64	4.200 (−4)	4.865 (+9)
1^e_0	61^o_1	13.871 91	3.087 (−4)	3.566 (+9)
1^e_0	60^o_1	13.894 76	1.149 (−5)	1.324 (+8)
1^e_0	59^o_1	13.943 44	5.158 (−5)	5.899 (+8)
1^e_0	58^o_1	13.945 63	1.952 (−5)	2.232 (+8)
1^e_0	57^o_1	13.957 20	1.174 (−4)	1.340 (+9)
1^e_0	56^o_1	13.996 82	1.189 (−4)	1.349 (+9)
1^e_0	55^o_1	14.004 36	9.948 (−5)	1.128 (+9)
1^e_0	54^o_1	14.008 99	2.818 (−4)	3.193 (+9)
1^e_0	53^o_1	14.017 00	3.365 (−4)	3.808 (+9)
1^e_0	52^o_1	14.042 76	1.320 (−3)	1.489 (+10)
1^e_0	51^o_1	14.047 72	1.004 (−4)	1.131 (+9)
1^e_0	50^o_1	14.066 68	1.317 (−5)	1.480 (+8)
1^e_0	49^o_1	14.080 15	8.581 (−5)	9.624 (+8)
1^e_0	48^o_1	14.089 19	3.071 (−4)	3.440 (+9)
1^e_0	47^o_1	14.091 81	1.991 (−6)	2.229 (+7)
1^e_0	46^o_1	14.107 71	4.439 (−5)	4.958 (+8)
1^e_0	45^o_1	14.120 35	4.482 (−4)	4.998 (+9)
1^e_0	44^o_1	14.145 86	1.285 (−5)	1.428 (+8)
1^e_0	43^o_1	14.156 24	2.574 (−4)	2.855 (+9)
1^e_0	42^o_1	14.164 99	4.758 (−6)	5.273 (+7)
1^e_0	41^o_1	14.184 17	7.814 (−5)	8.635 (+8)
1^e_0	40^o_1	14.190 81	1.252 (−6)	1.382 (+7)
1^e_0	39^o_1	14.203 08	1.630 (−6)	1.796 (+7)
1^e_0	38^o_1	14.207 47	5.930 (−5)	6.532 (+8)
1^e_0	37^o_1	14.247 24	4.640 (−6)	5.082 (+7)
1^e_0	36^o_1	14.255 15	7.714 (−5)	8.440 (+8)
1^e_0	35^o_1	14.267 24	4.627 (−6)	5.054 (+7)
1^e_0	34^o_1	14.285 80	5.342 (−8)	5.820 (+5)
1^e_0	33^o_1	14.293 43	1.647 (−5)	1.792 (+8)
1^e_0	32^o_1	14.299 66	2.027 (−5)	2.204 (+8)
1^e_0	31^o_1	14.310 04	7.542 (−6)	8.189 (+7)
1^e_0	30^o_1	14.326 85	5.127 (−6)	5.554 (+7)
1^e_0	29^o_1	14.337 13	6.547 (−6)	7.081 (+7)

Table 5 – *continued*

Level index lower	upper	λ (Å)	f_{ij}	A_{ji} (s^{-1})
1^e_0	28^o_1	14.353 32	7.163 (−5)	7.731 (+8)
1^e_0	27^o_1	14.367 98	9.178 (−5)	9.885 (+8)
1^e_0	26^o_1	14.398 59	1.657 (−6)	1.777 (+7)
1^e_0	25^o_1	14.406 12	8.682 (−6)	9.301 (+7)
1^e_0	24^o_1	14.435 26	1.757 (−6)	1.875 (+7)
1^e_0	23^o_1	14.488 12	3.125 (−5)	3.310 (+8)
1^e_0	22^o_1	14.490 38	3.117 (−5)	3.301 (+8)
1^e_0	21^o_1	14.514 39	8.704 (−7)	9.186 (+6)
1^e_0	20^o_1	14.571 13	1.469 (−6)	1.538 (+7)
1^e_0	19^o_1	14.609 99	1.157 (−5)	1.205 (+8)
1^e_0	18^o_1	14.618 37	8.970 (−7)	9.333 (+6)
1^e_0	17^o_1	15.227 86	1.795 (+0)	1.721 (+13)
1^e_0	16^o_1	15.374 88	1.383 (−1)	1.301 (+12)
1^e_0	15^o_1	15.479 99	6.003 (−1)	5.570 (+12)
1^e_0	14^o_1	15.538 14	1.701 (−2)	1.567 (+11)
1^e_0	13^o_1	15.572 87	6.211 (−3)	5.694 (+10)
1^e_0	12^o_1	15.608 17	7.247 (−3)	6.615 (+10)
1^e_0	11^o_1	15.655 54	2.533 (−2)	2.298 (+11)
1^e_0	10^o_1	15.745 90	2.410 (−3)	2.161 (+10)
1^e_0	9^o_1	15.779 71	4.131 (−2)	3.689 (+11)
1^e_0	8^o_1	15.799 84	1.287 (−4)	1.146 (+9)
1^e_0	7^o_1	15.901 79	1.991 (−4)	1.751 (+9)
1^e_0	6^o_1	15.978 80	1.256 (−3)	1.093 (+10)
1^e_0	5^o_1	16.008 89	5.987 (−2)	5.194 (+11)
1^e_0	4^o_1	16.046 49	1.058 (−2)	9.138 (+10)
1^e_0	3^o_1	16.151 78	1.277 (−5)	1.088 (+8)
1^e_0	2^o_1	16.195 18	4.040 (−5)	3.425 (+8)
1^e_0	1^o_1	16.266 14	1.669 (−4)	1.403 (+9)

in *set 1*) is not sufficient to achieve a reasonable accuracy for f values.

While comparing the *set 2* and *set 3* figures, one can see that agreement between f_L and f_V is much better in the case of wavefunction expansion having configurations with one and two electrons in the $n = 4$ shell. Nevertheless, while considering the differences between f_L values from these two sets, we note that they change by only a few per cent for the stronger lines (having $f_L > 10^{-3}$) and by no more than 10 per cent for the lines with $10^{-6} < f_L < 10^{-3}$. Therefore, we conclude that using the full set of configurations described in Section 2.2 allows us to achieve convergence for 2p–3*l* transition oscillator strengths, and to determine reliable atomic data. The addition of more excited configurations into the wavefunction expansion, such as $n = 5$ shell configurations or configurations with two electrons excited from the 2p shell, should not change the derived values of oscillator strengths significantly.

In Fig. 2 the velocity-form oscillator strengths log (f_V) are plotted against the length-form oscillator strengths log (f_L) for all lines from the 2p–3*l* transition array in Fe XV. Here we have two different arrays: transitions to the excited-state $J = 1/2$ levels (circles) and those to the $J = 3/2$ levels (triangles). Similarly to the previous figure, a comparison is made for the three different sets of CSFs for Fe XV, arranged using the same rules as for Fe XVI.

The pattern of f-value changes here is similar to the earlier case; the introduction of configurations with $n = 4$ electrons significantly changes the oscillator strength data from *set 1* to *set 2*. The agreement between f_L and f_V is better when a full set of configurations with one and two electrons in the $n = 4$ shell is included, as described in Section 2.2. Very good agreement between f_L and f_V can be achieved for all lines with $f_L > 5 \times 10^{-5}$, and for most of the weaker lines. There are some exceptions to this rule where

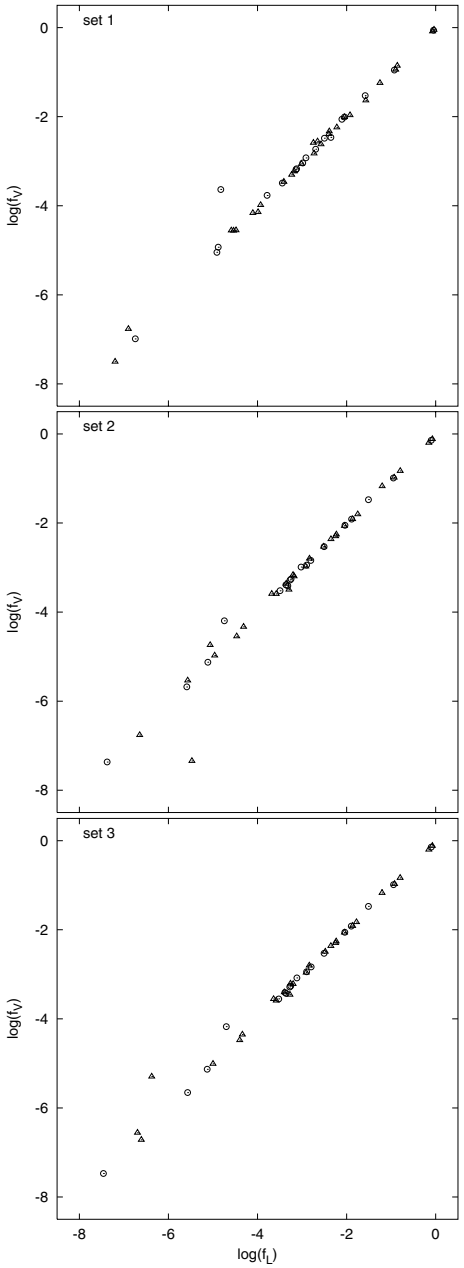

Figure 1. Comparison of the oscillator strengths in the length and velocity forms of the E1 transition operator for the Fe XVI ion calculated with different sets of CSFs.

the differences between the two forms is more evident, but these lines are comparatively weak and correspond to the transitions to the levels marked 39^o_1, 40^o_1, 42^o_1, 64^o_1, 65^o_1, 67^o_1, 68^o_1 and 74^o_1. As one can see from Table 3, the leading contributions to these levels come from the ^3L or ^5L terms of the $3p^2 3d$, $3s3d^2$ and $3d^3$ configurations, and therefore the E1 transitions to these terms are forbidden in pure *LS* coupling.

One of the possible ways to improve the accuracy of the calculated oscillator strengths would be a further increase of the CSF numbers in a wavefunction expansion. Although we can make only a very general quantitative estimate, we do not think that this extension will change the calculated f-values by more than 10 per cent. Therefore, we conclude that the atomic data presented here are of high

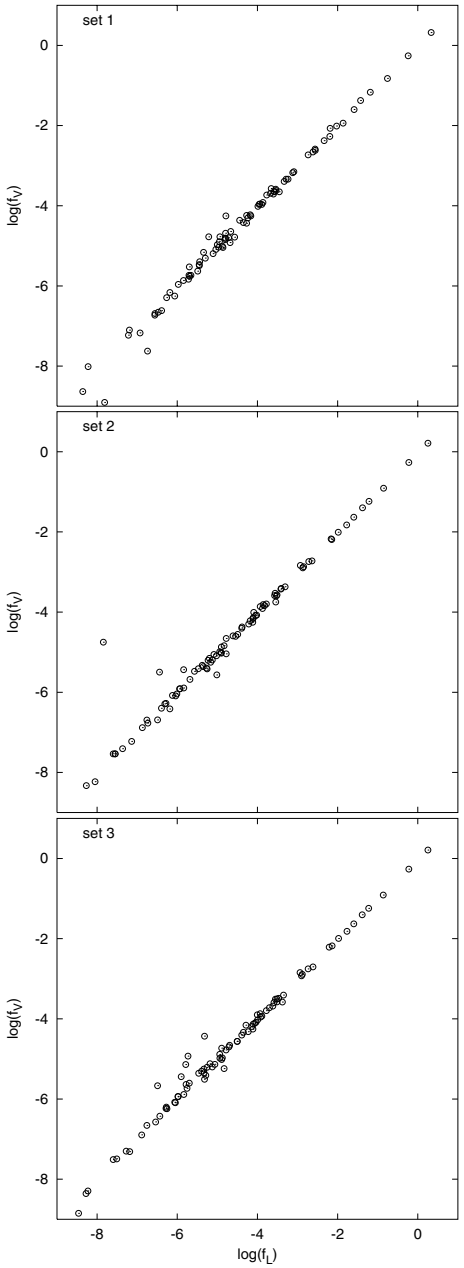

Figure 2. Comparison of the oscillator strengths in the length and velocity forms of the E1 transition operator for the Fe XV ion calculated with different sets of CSFs. Circles denote the 1/2–1/2 transitions and triangles denote the 1/2–3/2 transitions.

accuracy, and may be employed for the modelling of plasma X-ray spectra.

As in the case of oscillator strengths, we can perform convergence tests for the E1-transition wavelengths. In Table 6, we present transition wavelengths λ for the strongest lines ($f_L \geqslant 10^{-3}$) in Fe XVI and Fe XV obtained using all configurations described earlier (*set 3*) in the CSF expansion for wavefunction. Alongside, we present the percentage deviations $\delta\lambda_i(\%) = 100 \times (\lambda_i - \lambda)\lambda^{-1}$ for the wavelengths, obtained using truncated wavefunction expansions of *set 1* for the $\delta\lambda_1$ and *set 2* for $\delta\lambda_2$. It is quite evident from Table 6 that expansion of CSF basis leads to the convergence of the calculated transition wavelengths. In the case of Fe XVI, the average absolute value of $\delta\lambda_1 = 0.070\%$, whereas $\delta\lambda_2 = 0.015\%$ for the

Table 6. Electric dipole transition wavelengths λ (in Å) for selected lines of the Fe XVI and Fe XV ions and the deviations $\delta\lambda_i$ (in per cents) from the corresponding line wavelengths calculated with different sets of CSFs.

Level index				
lower	upper	λ(Å)	$\delta\lambda_1$ (%)	$\delta\lambda_2$ (%)
		Fe XVI		
$1^e_{1/2}$	$1^o_{1/2}$	16.965 14	−0.187	0.004
$1^e_{1/2}$	$2^o_{1/2}$	15.837 34	0.027	0.002
$1^e_{1/2}$	$3^o_{1/2}$	15.748 02	0.050	0.002
$1^e_{1/2}$	$4^o_{1/2}$	15.626 60	0.034	0.001
$1^e_{1/2}$	$5^o_{1/2}$	15.586 91	−0.064	0.003
$1^e_{1/2}$	$7^o_{1/2}$	15.457 84	−0.042	0.001
$1^e_{1/2}$	$8^o_{1/2}$	15.384 17	−0.082	0.001
$1^e_{1/2}$	$11^o_{1/2}$	15.083 31	−0.258	−0.002
$1^e_{1/2}$	$1^o_{3/2}$	17.246 21	−0.190	0.004
$1^e_{1/2}$	$2^o_{3/2}$	15.843 53	0.029	0.001
$1^e_{1/2}$	$3^o_{3/2}$	15.793 10	0.034	0.002
$1^e_{1/2}$	$5^o_{3/2}$	15.603 74	0.048	0.002
$1^e_{1/2}$	$6^o_{3/2}$	15.569 17	−0.022	0.003
$1^e_{1/2}$	$8^o_{3/2}$	15.512 47	0.047	−0.010
$1^e_{1/2}$	$10^o_{3/2}$	15.470 88	−0.049	0.002
$1^e_{1/2}$	$11^o_{3/2}$	15.408 44	−0.067	0.000
$1^e_{1/2}$	$12^o_{3/2}$	15.321 19	−0.074	0.000
$1^e_{1/2}$	$13^o_{3/2}$	15.282 52	−0.057	0.003
$1^e_{1/2}$	$14^o_{3/2}$	15.204 39	−0.097	−0.002
$1^e_{1/2}$	$15^o_{3/2}$	15.153 71	−0.159	−0.001
$1^e_{1/2}$	$16^o_{3/2}$	14.996 28	−0.181	−0.004
$1^e_{1/2}$	$27^o_{3/2}$	13.658 53	−0.162	−0.027
		Fe XV		
1^e_0	4^o_1	16.046 49	−0.064	0.008
1^e_0	5^o_1	16.008 89	−0.069	0.005
1^e_0	6^o_1	15.978 80	−0.035	0.009
1^e_0	9^o_1	15.779 71	−0.070	−0.004
1^e_0	10^o_1	15.745 90	−0.118	0.004
1^e_0	11^o_1	15.655 54	−0.058	−0.001
1^e_0	12^o_1	15.608 17	−0.131	0.000
1^e_0	13^o_1	15.572 87	−0.067	−0.013
1^e_0	14^o_1	15.538 14	−0.105	0.000
1^e_0	15^o_1	15.479 99	−0.210	−0.001
1^e_0	16^o_1	15.374 88	−0.165	−0.002
1^e_0	17^o_1	15.227 86	−0.314	−0.005
1^e_0	52^o_1	14.042 76	−0.122	−0.023
1^e_0	66^o_1	13.770 74	−0.235	−0.023
1^e_0	69^o_1	13.616 06	−0.305	−0.030

$J = 1/2 - 1/2$ transitions and $\delta\lambda_1 = 0.063\%, \delta\lambda_2 = 0.012\%$ for the $J = 1/2 - 3/2$ transitions. In case of Fe XV, the corresponding values are $\delta\lambda_1 = 0.099\%, \delta\lambda_2 = 0.022\%$. The maximum value of difference between *set 2* and *set 3* results is 0.1% for both Fe XVI and Fe XV ions.

It is not possible to determine an absolute value of the transition wavelength λ accuracy obtained in our ab initio calculation. We can only estimate that calculated energy differences ΔE are accurate to about 0.05−0.06 au. For the $2p - 3l$ transitions considered here, it would give an estimated wavelength accuracy of 0.2%, twice the actual deviation between sets 2 and 3.

5 CONCLUSIONS

We have presented extensive calculations of energy levels, transition wavelengths, absorption oscillator strengths and emission transition probabilities for Fe XVI and Fe XV. Atomic data for the

electric dipole transitions representing the inner-shell transition array 2p–3*l* were determined using the configuration-interaction method implemented in the CIV3 code. As a result of the lack of available previous atomic data, it was not possible to make a comparison of our calculations with experimental values or with the results of other calculations. However, our results indicate satisfactory agreement between length and velocity oscillator strength forms. Therefore, we conclude that the data are generally of high accuracy, and suitable for applications in plasma X-ray spectral modelling.

ACKNOWLEDGMENTS

This work was supported by EPSRC and PPARC, and also by NATO Collaborative Linkage Grant CLG.979443.

REFERENCES

Ballantyne D.R., Ross R.R., Fabian A.C., 2002, MNRAS, 336, 867
Behar E., Sako M., Kahn S.M., 2001, ApJ, 563, 497
Clementi E., Roetti C., 1974, At. Data Nucl. Data Tables, 14, 177
Ferland G.J., Korista K.T., Verner D.A., Ferguson J.W., Kingdon J.B., Verner E.M., 1998, PASP, 110, 761
Foord M.E. et al., 2001, in Ferland G., Savin D.W., eds, ASP Conf. Ser., Vol. 247, Spectroscopic Challenges of Photoionized Plasmas. Astron. Soc. Pac., San Francisco, p. 117
Hibbert A., 1975, Comput. Phys. Commun., 9, 141
Hibbert A., 1996, Physica Scripta, T65, 104
Hibbert A., Glass R., Froese Fischer C., 1991, Comput. Phys. Commun., 64, 455
Kallman T., Bautista M., 2001, ApJSS, 133, 221
Kaspi S., Brandt W.N., Netzer H., Sambruna R., Chartas G., Garmire G.P., Nousek J.A., 2000, ApJ, 535, L17
Rose S.J., 1998, J. Phys. B: At. Mol. Opt. Phys., 31, 2129
Schurch N.J., Warwick R.S., 2002, MNRAS, 334, 811
Yang Y., Wilson A.S., Ferruit P., 2001, ApJ, 563, 124

This paper has been typeset from a TEX/LATEX file prepared by the author.